EFDA–JET–PR(10)05

K.V. Beausang, S.L. Prunty, M.J. Walsh, E de La Luna, R. Scannell,
M. Beurskens, M. Maslov, I. Balboa and JET EFDA contributors

Investigation of the TS/ECE Temperature Measurement Discrepancy at JET Using the Core LIDAR TS Diagnostic

Investigation of the TS/ECE Temperature Measurement Discrepancy at JET Using the Core LIDAR TS Diagnostic

K.V. Beausang[1], S.L. Prunty[1], M.J. Walsh[2], E de La Luna[3], R. Scannell[2], M. Beurskens[2], M. Maslov[2], I. Balboa[2] and JET EFDA contributors*

JET-EFDA, Culham Science Centre, OX14 3DB, Abingdon, UK

[1]EURATOM/DCU, Department of Electrical & Electronic Engineering, University College Cork, Cork, Ireland
[2]EURATOM-CCFE Fusion Association, Culham Science Centre, OX14 3DB, Abingdon, OXON, UK
3Asociación EURATOM-CIEMAT, Laboratorio Nacional de Fusion, E-28040 Madrid, Spain
** See annex of F. Romanelli et al, "Overview of JET Results",*
(Proc. 22 [nd] IAEA Fusion Energy Conference, Geneva, Switzerland (2008)).

Preprint of Paper to be submitted for publication in
Plasma Physics and Controlled Fusion

ABSTRACT.

The present work is motivated by a long standing discrepancy between the electron temperature measurements of Thomson Scattering (TS) and Electron Cyclotron Emission (ECE) diagnostics for plasmas with strong auxiliary heating observed at both JET and TFTR, where in some cases the TS electron temperature measurements can be 15 - 20% lower than ECE measurements. This problem is a significant concern for the fusion community as highlighted in [1]. Recent analysis based on ECE results at JET have suggested that the assumption of a Maxwellian electron velocity distribution may not be valid under the influence of high levels of NBI and ICRF heating. Such results have indicated distortions to the low-energy part of the distribution, rather than simply the generation of a tail of fast electrons. A non-Maxwellian distribution function was proposed by Krivenski [2, 3], which appeared to resolve the difference between the ECE and TS central temperatures but a physical mechanism responsible for such behaviour was not identified. In this paper, the JET core LIDAR TS measurements have been utilised in an attempt to detect the presence of non-Maxwellian distributions. As part of this work, a model was developed to evaluate the theoretical number of scattered photoelectrons in each spectral bin of the core LIDAR TS system for an arbitrary electron distribution. Using this model, the experimental measurements of the LIDAR system, under numerous heating conditions, have been compared with theoretical data simulated from the non-Maxwellian bulk distribution and a 'high energy tailed' Lorentzian distribution. In this way, efforts were made to isolate the most likely velocity distribution for certain heating conditions and determine if any detected deviations from a Maxwellian could be related to the TS/ECE discrepancy. Additional analysis was carried out to identify possible calibration inaccuracies with the LIDAR system and determine if their effect could contribute to the TS/ECE discrepancy.

1. INTRODUCTION

Incoherent Thomson scattering (TS) has become a standard diagnostic for electron temperature T_e and density n_e measurements in modern tokamaks. A high power laser is passed into the plasma and as it propagates through the plasma, light is scattered from the electrons in its path. Through detailed analysis of the scattered light, the electron temperature and density along the laser path can be determined. Under most conditions, it can be assumed that the electron velocity distribution can be represented by a relativistic Maxwellian distribution and this assumption is utilised to evaluate the electron temperature and density from the scattered light. However, recent experiments [3, 4] have suggested that this hypothesis may be violated in the presence of high auxiliary heating. Firstly, it is accepted that lower hybrid heating generates a population of fast electrons, thus producing a tail on the Maxwellian distribution. However, most of the high energy electrons are beyond the energy range measured by TS systems and so theoretically will not significantly affect the temperature and density results. Secondly, it has been proposed [2, 3], that the low-energy part may deviate from a Maxwellian under particular conditions but a possible mechanism for such a distortion has not been identified. Since TS diagnostics detect light mainly from low energy electrons, such a Maxwellian

distortion may have consequences on the TS electron temperature measurements.

In [3], a non-Maxwellian bulk distribution function was derived by analysing the ECE spectra measured by the Michelson spectrometer at JET over several harmonics for a specific TS/ECE discrepant case. For this plasma shot, both the second and third harmonics (both X-mode and optically thick) were studied, thus providing two independent temperature profile measurements. Their temperature profiles were inconsistent and therefore, indicated an anomaly e.g. the presence of a non-Maxwellian distribution. A model non-Maxwellian bulk distribution function with a flattening in the low energy region was then proposed, which made it possible to not only theoretically reproduce the measured ECE spectrum but also to resolve the difference between the ECE and TS central temperatures.

The aim of this paper is to determine whether or not a non-Maxwellian bulk distribution function can be identified from the experimental results of the LIDAR TS system for some of the examples where a temperature discrepancy has been observed. This will be performed by comparing experimental data with those simulated from the non-Maxwellian bulk distribution function. In addition, the experimental data is compared with data simulated for a generalized Lorentzian electron distribution [5] using a least squares method to isolate the best fit in each case. Simulations were first carried out for a few cases which were representative of purely ohmic heating to verify the assumption of a Maxwellian distribution for this condition and as a method to validate the model. The analysis was then repeated for a number of discrepant and non-discrepant plasma shots and the most probable electron distribution for each was identified.

The remainder of the paper is arranged as follows. In section 2, details of the TS/ECE discrepancy as well as the recent work that has been done in the area are discussed. The principles of Thomson scattering diagnostics and the experimental arrangement of the LIDAR TS diagnostic at JET are summarised in section 3. The Lorentzian distribution, the non-Maxwellian distribution and details of the analysis performed are discussed in section 4. In section 5, possible calibration issues with the LIDAR TS diagnostics are discussed as well as their consequences on the temperature estimations and the detection of non-Maxwellian behaviour. Conclusions are presented in the final section.

2. THE TS/ECE TEMPERATURE DISCREPANCY

The discrepancy between ECE and TS temperature diagnostics is clearly illustrated in Figure 1, where for both JET and TFTR, systematic discrepancies are observed for temperatures exceeding 5- 6 keV. The discrepancy at JET can be characterised by two features; firstly, the disagreement in temperature is present only in the plasma core and secondly, for the discrepant plasma shots analysed thus far, the measured ECE spectra are inconsistent with that of a Maxwellian electron distribution, where the peak intensity of the third harmonics are less than the second despite both harmonics being optically thick, as portrayed in Figure 2 for discrepant Pulse No: 53505.

Work was carried out by E. de la Luna et al [7] to investigate the role of different plasma parameters

on the observed discrepancy by compiling a list of high performance discharges from the period 2004-2006, some of which portrayed the TS/ECE discrepancy. All of these discharges were obtained using the so called hybrid scenario with dominant electron heating containing a combined NBI and ICRH heating often greater than 20MW. In 2004, the hybrid regime was developed at JET using Lower Hybrid (LH) heating in the order of 1MW during the ramp up phase to optimise the plasma current profile, followed by the application of NBI and ICRH heating. Central electron temperatures in the range 5-8 keV and electron densities of 3-4 $\times 10^{19}\,\mathrm{m}^{-3}$ can be achieved in this way. Although the plasma conditions and heating scenario were very similar, the experiments performed in 2006 utilised a slightly different ICRH heating procedure. In 2004, the hydrogen concentration relative to deuterium concentration was approximately 3% whereas in 2006, this was raised to a higher level of 8% in an attempt to minimise fast ion losses [7].

On examination of the ECE spectra from these discharges, a clear difference between the 2004 and 2006 cases was observed, despite such similar plasma conditions. This can be seen in Figure 3, where the ECE spectra and TS/ECE temperatures profiles from each campaign are shown. It can be seen that the TS and ECE profiles agree quite well for the plasma Pulse No's: 68383 (2006) but for 62696 (2004), a large disagreement ($\approx$15%) is shown in the central region. In addition, the ECE spectrum for Pulse No: 68383 exhibits Maxwellian behaviour where both the second and third harmonics are approximately equal in intensity. On the other hand, this is clearly not the case for Pulse No:62696, which indicates non-Maxwellian behaviour. Note that for these plasma conditions, the third harmonic will also be optically thick giving an additional measurement of the temperature profile and should match that of the second harmonic provided the distribution function is Maxwellian. In fact, for the discrepant cases analysed, it appears that the temperature profiles determined from the third harmonic agree much better with the TS profiles than those from the second harmonic.

In [7], it is suggested that the electron temperature discrepancy is correlated with the appearance of a high energy tail in the ion distribution function, which is caused by the low hydrogen concentration as the fraction of the ICRH absorbed by the deuterium ions is inversely proportional to the hydrogen concentration. It is proposed in [7] that the effect of this high energy tail may cause a distortion to the low energy region of the electron distribution and thus cause the temperature discrepancy. In the past, numerous reasons for the discrepancy have been suggested including calibration issues and the spatial resolution of the diagnostics. However, recent analysis [6] has eliminated calibration issues with the ECE measurements and problems with spatial resolution as possible causes and indicated that the presence of non-Maxwellian electron distributions is the most probable reason for the discrepancy.

3. THOMSON SCATTERING DIAGNOSTICS

3.1. SCATTERED POWER

The formula for the incoherent Thomson scattered power from a volume of electrons per unit solid angle Ω, per unit angular frequency ω_s, is given by [8]

$$\frac{d^2\bar{P}}{d\ d\omega_s} = r_e^2 \int_V \langle S_i \rangle d^3 r \int \left| 1 - \frac{(1-\cos\ )\ e^2}{(1-\cos\ _1)(1-\cos\ _2)} \right|^2 \times \left| 1 - \frac{(1-\cos\ _1)}{(1-\cos\ _2)} \right|^2 (1-\ ^2) f(\ ) \delta(\kappa \cdot\ -\ ) d^3 \quad (1)$$

where r_e is the classical electron radius, θ is the scattering angle, $\hat{\boldsymbol{e}}$ is a unit vector in the direction of the incident electric field and $\langle S_i \rangle = (1/2)\in_0 c\ |\vec{E}_i|^2$ is the mean incident Poynting vector. θ_1 and θ_2 are the angles between the electron velocity and the incident and the scattered wave vectors, respectively. β_e, $\beta_{\cos}\theta_1$, and $\beta_{\cos}\ \theta_2$ are the components of the electron velocity in the direction of the incident electric field, incident and scattered radiation wave vectors. f (β) is the electron velocity distribution, $\boldsymbol{k} = \boldsymbol{k_s} - \boldsymbol{k_i}$ and $\omega = \omega_s - \omega_i$ with $\boldsymbol{k_i}$ and ω_i being the wave vector and frequency of the incident radiation and $\boldsymbol{k_s}$ and ω_s being the scattered radiation. Note that this is specified for the condition where the electric field $\hat{\boldsymbol{e}}$ is perpendicular to the scattering plane and only the component of scattered field in the direction of $\hat{\boldsymbol{e}}$ is measured. In Equation (1) all relativistic effects have been included. In modern tokamaks, including JET, temperatures exceeding 10keV have been achieved and temperatures as high as 40keV are predicted for next step devices. At these temperatures, the electron velocities are a substantial fraction of the velocity of light causing, firstly, an increasing 'blue shift' in the scattered spectrum and secondly, a reduction in the spectral intensity due to a change in polarization of the scattered light [8, 9]. In most cases, the plasma will be in a state of local thermal equilibrium and so the electron distribution $f(\beta)$ can be represented by a relativistic Maxwellian providing a single temperature measurement. In general, it is in fact the number of scattered photons that is measured rather than the scattered power and in this case, we must account for the fact that the scattered photons have different energies to that of the incident and so we must multiply Equation (1) by ω_s / ω_i [8].

3.2. THE JET CORE LIDAR TS SYSTEM

The core LIDAR (Light Detection and Ranging) TS system uses the time of flight technique to spatially resolve electron temperature and density measurements within the plasma using a single set of detectors. The system uses a 694.3nm Ruby laser with a 1J pulse energy, 300ps pulse duration and a repetition rate of 4Hz, together with 450ps FWHM MCP photomultiplier detectors and 1 GHz bandwidth digitizers to yield a spatial resolution of approximately 12cm across the JET plasma ($\approx$ 2m). The spatial resolution δL can be calculated by $\sqrt{\tau_D^2 + \tau_D^2}$, where τ_L is the laser pulse duration and τ_D is the combined response time of the detection system. A six channel interference edge filter polychromator spanning a wavelength range 385–830nm provides a theoretical temperature measurement range of 0.3–20keV with a typical accuracy of 10% [10]. The photomultiplier detectors are gated to minimise stray light scattered from the centre column. A ruby notch filter is also used in one of the spectral channels. The solid angle of collection is $\approx 5.5\times10^{-3}$ sr and the transmission is approximately 15% over the detectable range. A schematic of the system layout is shown in Figure

4 and more details can be found in [10, 11].

3.3. MEASURING TEMPERATURE AND DENSITY

In order to determine the electron temperature T_e and density n_e profiles, a non-linear least squares fit is performed every 5cm through the plasma, where the scattering location is resolved using the time of flight method. Six data points are provided by the six spectral channels, whose scattered signals, in number of photoelectrons per second, can be written as,

$$n_s = n_e\, n_{laser}\, r_e^2 \Delta\Omega\, L \int \; _e(\; _s)\, \frac{S(\; _s, T_e, \;)}{\; _i}\; d\; _s \tag{2}$$

where $\phi_i(\lambda_s)$ is the spectral transmission of the optical filter *i* incorporating the filter quantum efficiency, n_{laser} is the number of photoelectrons in the scattered laser pulse, $\Delta\Omega$ is the solid angle of collection and L is scattering length. The spectral transfer functions for the filters are illustrated in Figure 5 with a spectral resolution of 5nm. The spectral channels are designed to divide the spectrum such that at least two channels will have high signal levels for all temperatures, which will enable good temperature estimation. For low T_e, the scattered spectrum is symmetric about the laser wavelength and spectral channels on either side will reduce measurement errors at these temperatures. However, a notch filter is required around the laser wavelength as stray light would dramatically effect results. For temperatures below 10keV, the width of the scattered spectrum increases with electron temperature and in modern spectrometer designs, the channels become increasingly broader for higher temperature measurements so as to divide the spectrum between at least two channels and thus achieve low fitting errors. As the temperature is increased further, the spectrum narrows and so the channels also narrow. In Figure 6, the signal levels in each spectral channel over a large range of temperatures are illustrated. It shows that the scattered spectrum is divided adequately between channels to allow accurate temperature estimation for the desired temperature range.

In the LIDAR fitting routine, a look-up table is generated containing the theoretical signals f_i for each spectral filter *i* for a large range of temperatures in steps of approximately 100eV and for a constant density of 1×10^{19} m^{-3}. This involves the numerical integration of the fully relativistic scattered spectrum, based on the Maxwellian velocity distribution, convoluted with the spectral transfer functions of the six channels. Note that although there will be a slight deviation in the scattering angle with scattering position, its effect is negligible.

A least square fit between the theoretical signals f_i and the measured signals y_i, given by the instantaneous light level minus the average background plasma light, is then performed to determine the electron temperature and density as shown below,

$$\chi^2 = \sum_{i=1}^{n} \frac{(y_i - f_i n_e)^2}{\sigma_i^2} \tag{3}$$

where σ_i is the signal standard deviation in channel *i*, which is calculated from the total light level,

n is the number of spectral channels and ne is the density in 1×10^{19} m^{-3}. The actual final fitted temperature is then found by locating the minimum of the parabola joining the three smallest chi-square values. The maximum and minimum values of temperature are determined as those which increase the chi-square by one from its minimum value [12]. The final value of density is derived by accounting for the variation in solid angle along the laser line of sight and the actual measured laser energy.

4. CHI-SQUARE ANALYSIS USING NON-MAXWELLIAN ELECTRON VELOCITY DISTRIBUTIONS

4.1. PROCEDURE

As discussed previously, the electron temperature is determined from the Thomson scattered signals based on the assumption of a Maxwellian plasma. It has been suggested that a deviation of the electron distribution from a Maxwellian may cause the observed discrepancy between ECE and TS diagnostics under certain heating conditions. A model was developed to evaluate the theoretical Thomson scattered signals of the core LIDAR TS system at JET for an arbitrary electron distribution, allowing theoretical TS signals based on non-Maxwellian distribution functions to be fitted to the experimental signals in an attempt to investigate the existence of non-Maxwellian plasmas under certain heating conditions. However, rather than selecting data for a single radial point and time slice, the analysis was performed at the plasma centre over the entire duration of the LIDAR measurement period as conclusions based on a single data set can be misleading due to the significant scatter in the LIDAR data. The resultant chi-square values were recorded and analysed in an attempt to isolate the most probable electron distribution for each plasma condition. The shots analysed included purely ohmic shots, which could be used to validate the model as the electron distribution should be Maxwellian under these conditions. Then a number of plasma discharges that had been previously highlighted as portraying a discrepancy between the TS and ECE measurements were analysed. Finally, sample shots with high heating conditions but not portraying such a temperature disagreement were analysed.

Two different distribution functions were used as the non-Maxwellian distributions. Firstly, a generalized Lorentzian was used to model a distribution with a high energy tail and a distribution suggested by Krivenski [3] was used to model a non-Maxwellian bulk distribution.

4.2. THE GENERALIZED LORENTZIAN DISTRIBUTION

A suitable representation of a 'high energy tailed' distribution was required as part of this analysis. A superposition of Maxwellians could have been used but it was decided that a generalized Lorentzian would be better as it contains fewer fitting parameters and can be used to model a larger range of distributions. The generalized Lorentzian has the form of a power law distribution $f(E)-E^{-k}$, where an appropriate relativistic form of the generalized Lorentzian is given by [5],

$$f_L(p) = \frac{3\,\alpha^{\frac{3}{2}}}{4\pi\,(m_e c)^3 \kappa^{\frac{5}{2}}} \left[B\left(\frac{5}{2}, \kappa - 3\right) {}_2F_1\left(\frac{5}{2}, -\frac{3}{2}; \kappa - \frac{1}{2}; \frac{4\alpha - \kappa}{4\alpha}\right)\right]^{-1} \left(1 + \frac{2\alpha\,(\gamma - 1)}{\kappa}\right)^{-\kappa} \tag{4}$$

where p and m_e are the momentum and mass of the electron, $\gamma = [1 + p^2/(m_e c)^2]^{1/2}$, $\alpha = m_e c^2/(2T_e^*)$ and T_e is the bulk temperature. ${}_2F_1$ is the Gauss Hypergeometric function, B is the beta function and κ is the spectral index, which must be greater than four for a finite average energy [5]. κ describes the "extent" of the high energy tail. Note that as $\kappa \to \infty$, the distribution becomes a Maxwellian. In Figure 7, the generalized Lorentzian distribution is shown for a number of κ values.

The scattered spectrum based on the Lorentzian distribution can be calculated numerically or using an analytical approximation as derived in [5], which has a peak relative error of less than 0.3% at $T_e^* = 30$keV for a 90° scattering angle. Since the analytical formula was sufficiently accurate within the desirable temperature range, it was used in the regression model. The spectral density functions for the Lorentzian distribution with $\kappa = 5$, 10, 20 at $T_e^* = 10$keV for LIDAR scattering are shown in Figure 8. It shows that the high energy tail causes a 'blue shift' in the spectral peak when compared with the Maxwellian and the spectral shape itself becomes broader.

In the chi-square analysis, the Lorentzian model is fitted to the experimental TS signals and the value of κ which obtained the lowest chi-square is recorded along with its corresponding chi-square value. However, for the purpose of simplicity only the $\kappa = 5$ values will be used in the subsequent graphs. This allows one to clearly highlight a difference between Maxwellian and Lorentzian behaviour. In addition, it was noticed that during levels of high heating, the difference between the $\kappa = 5$ chi-square value and the actual minimum chi-square value was small and did not provide any additional information regarding the electron distribution.

4.3. THE NON-MAXWELLIAN BULK DISTRIBUTION

A representation of a non-Maxwellian bulk distribution was proposed in by V. Krivenski in [3] but the mechanism necessary to achieve this bulk distortion was not established. This distribution was generated in order to match the theoretical and experimental ECE spectra over several harmonics for a particular TS/ECE discrepant case observed at JET (Pulse No: 53689 at 9.71s). In order to fit to the second and third harmonics, it was necessary to alter the distribution in the energy range of the 2nd harmonic, i.e. where $u \approx 1-1.5$ as shown in Figure 9, where $u = p/u_{th}$ and $u_{th} = \sqrt{m_e T_e}$. However, it is then necessary to alter the distribution in the very low energy region to ensure the normalisation condition, $\int_0^\infty 4\pi u^2 f(u) du = 1$ is satisfied. The exact form of the distribution function could not be attained directly and instead a sampling of the image given in [3] was performed [13]. Despite this approximation, good agreement betweenthe electron distribution shown below and that given in [3] is observed.

An analytical form of the distribution would be necessary to minimise computational intensity in the fitting routine. A sufficiently accurate representation of the distribution was created and is given by:

$$F(u) = \begin{cases} du^4 + eu^3 + fu^2 + g, & 0 < u < 1.423 \\ a\,exp[bu^2 + cu], & 1.423 < u < \end{cases} \quad (5)$$

where $a = 0.0664$, $b = -0.444$, $c = -0.188$, $d = -0.0122$, $e = 0.0132$, $f = -0.01135$, $g = 0.0556$. When deriving the analytical form of the distribution, an additional constraint was to ensure that the integral of the distribution over the entire energy range was as close to unity as possible. The use of an analytical distribution function introduces a $\approx 0.3\%$ peak relative error in the spectrum at a scattering angle of π radians for $T_e^* = 20$keV. However, since the original distribution was artifically created, this accuracy is sufficient for all analyisis. It must also be stated that since this distribution is composed of the two functions, a discontinuity exists at the point of intersection and will therefore not represent a real distribution. Despite this, it can still be used as a representation of a non-Maxwellian bulk distribution as this discontinuity will not cause a signficant effect to the shape of the scattered spectrum.

A comparison of the scattered spectra for the Maxwellian and non-Maxwellian bulk electron distributions at 10keV and for a scattering angle of π radians is illustrated in Figure 10. It shows that for the non-Maxwellian spectrum, the 'blue shift' in the spectral peak is decreased and the spectrum is narrower. This is in complete contrast to the Lorentzian spectrum, which is expected from the shape of the distributions.

4.4. CHI-SQUARE ANALYSIS RESULTS

The electron distribution functions discussed in the previous section were used in a model that was developed to evaluate the theoretical number of scattered photoelectrons in each spectral channel for the JET core LIDAR TS system for an arbitrary distribution. These theoretical signals were then fitted to the experimental LIDAR signals to estimate the temperature and density if such a distribution were present in the plasma. However, rather than concentrating on the temperature or density measurements, the behaviour of the chi-square in each fit was monitored. This enabled one to determine deviations in the electron distribution from a Maxwellian. These fits were carried out at the centre radial point ($r \approx 3.0$m) for each time point during the LIDAR measurement period.

4.4.1. Ohmic Heating Cases

As a method of model validation, the chi-square analysis was performed for a number of purely ohmic shots including Pulse No's: 69300, 75100 as shown in Figure 11, where the theoretical signals based on a pure Maxwellian should be the best fit at all times. These shots were heated entirely by a plasma current $I_p \approx 2$MA, reaching central temperatures of 2keV and densities of 3×10^{19} m^{-3}. In Figure 11 the relative chi-squares values are plotted, which were calculated by:

$$\chi_{rel} = \frac{\chi^2 - \chi^2_{Maxwell}}{\chi^2_{Maxwell}} \quad (6)$$

This means that the chi-square value for each fit is plotted relative to its corresponding Maxwellian value. Therefore, the blue zero line on the graphs represents theMaxwellian and if the other distributions achieve a lower χ^2 (i.e. a better fit) than the Maxwellian, it shall be below this line. The results show that the Maxwellian is almost exclusively the best fit distribution, indicating that the assumption of a Maxwellian distribution is verified during ohmic heating as no deviation from Maxwellian behaviour is detected. It is worth mentioning that on occasion either the Lorentzian or non-Maxwellian bulk distribution may for an instant be a better fit than the Maxwellian even for ohmic conditions, however such behaviour is never sustained and is more than likely due to the noisiness of the LIDAR data. Note also that the non-Maxwellian bulk chi-squares are much closer to the Maxwellian chi-squares than the Lorentzian values. This is expected from the comparison of the three different spectra.

4.4.2. TS/ECE Discrepancy Cases Plasma shots, which were previously
highlighted as containing a TS/ECE discrepancy were analysed. These included Pulse No's: 62693 and 62695, which are from the list of hybrid scenario discharges from 2004 as discussed in section 2 with non-Maxwellian ECE spectra. These shots were heated primarily with more than 8 MW of NBI and over 4 MW of ICRH where temperatures of $\approx$ 8keV and densities of $3 \times 10^{19}\,\mathrm{m}^{-3}$ were reached. Pulse No's: 62695 is also heated by 0.8 MW LH heating. The results of the chi-square analysis are shown in Figures 12(a) and 13(a).

Taking Pulse No: 62695 as an example, Figure 13(a) shows that during the period 1–8 secs, before the NBI+ICRH combination is applied, the Maxwellian distribution is the best fit at all times as for the purely ohmic shots. However, once the auxiliary heating is applied (8-16s), a clear change in the Maxwellian the chi-square values is observed and the Maxwellian is no longer the best fit at all times. Once the heating is turned off again, we revert back to ohmic conditions and the Maxwellian is again the best fit. During the additional heating phase, it is no longer possible to consistently determine the best fit. This would imply that either a deviation from a Maxwellian plasma is observed, where the exact form of the distribution is neither of the non-Maxwellian distributions used here or that it is not possible to distinguish between the three distributions at high temperature using the LIDAR data. Similar trends are observed for Pulse No: 62693, however a clear transition from ohmic to heating phase is less obvious from the non-Maxwellian bulk results.

4.4.3. TS/ECE Non-Discrepancy Cases
Finally, plasma shots which did not portray a TS/ECE discrepancy but have strong auxiliary heating applied were analysed. These included shots from the list of hybrid scenario discharges from 2006 as discussed in section 2. These shots were heated with NBI > 8MW and ICRH > 7MW with low levels of LH heating. Central temperatures greater than 9keV were reached with densities of $3{\times}10^{19}$ m^{-3} often achieved. However, the chi-square results for these shots were inconclusive as it was difficult to identify whether Maxwellian or non-Maxwellian behaviour was being observed during

either ohmic or auxiliary heating phases, as shown in Figure 14(a). It should be noted that the inconclusive results were contributed to, by the fact that the 2006 TS results contain only half the time points as the earlier results because the laser was set to operate at half the normal repetition rate. It was hoped that by comparing the 2004 and 2006 discharges that a conclusion regarding the TS/ECE discrepancy could be attained due to the similarity of the heating methods but this was not possible given these results.

A number of additional high performance shots were analysed in an effort to locate a "non-discrepant" discharge whose chi-square behaviour could be analysed with confidence. These included Pulse No's: 78098 and 75411 and the results of the chi-square analysis are shown in Figures 15(a) and 16(a). These shots were predominantly heated with more than 15MW NBI and temperatures over 6 keV and densities of 8×10^{19} m^{-3} are achieved. As with the discrepancy case, the results again show a clear change in the chi-square behaviour during the additional heating phase. In particular, looking at the ohmic phase of these shots, the Maxwellian is almost exclusively the best fit at all time points and this is clearly not the case during the heating phase. During the heating phase it is again difficult to consistently identify the best fit distribution. Since the change in chi-square behaviour is observed for both discrepant and non-discrepant shots, then this behaviour during heating is not related to the temperature discrepancy.

There are a number of possible reasons why the best fit distribution cannot be determined at high temperatures. Firstly, there may be calibration issues with high temperature spectral channels. However, some analysis of the LIDAR calibration has been carried out, as is described in section 5, and although some minor inaccuracies have been identified, the results of the chi-square analysis should not be affected. Secondly, it may be possible that non-Maxwellian distributions are detected for all high temperature cases but this contradicts the ECE results for the non-discrepancy cases, whose ECE spectra are consistent with those of a Maxwellian plasma. Finally, which seems the most plausible is that at high temperatures the tail of the scattered spectrum is no longermeasured as the tail is beyond the minimum wavelength detected by the LIDAR system. As a result, the theoretical spectra based on the different distributions can easily fit to one side of the experimental spectrum and a consistent best fit distribution cannot be determined. This would also explain why there is a very small difference between chi-square values over a large range of kappa during the heating phase, despite such a large change in the size of the high energy tail.

As a simple test, the chi-square analysis of ohmic Pulse No: 69300 and 75100 was repeated, but with the high temperature spectral channels five and six removed from the fit, so that the tail of the scattered spectrum is not used. A significant change in the chi-square behaviour is observed as shown in Figure 17 below when compared with Figure 11. The results show that the model cannot consistently determine that the Maxwellian is the best fit when channels five and six are removed from the fit. From these ohmic cases shown, it may be concluded that the reason for the inability to determine the best fit for the high performance shots during the heating phase, is because at high temperatures we are no longer measuring the tail of the spectrum as channels five and six have high

signal levels at these temperatures. The results would indicate that additional spectral channels beyond the wavelength range of channel six may be necessary in the LIDAR system in order to measure the tail of the scattered spectrum and therefore accurately determine the electron distribution at high temperatures,

4.5. TEMPERATURE ESTIMATIONS

In Figure 18(a), the fitted temperature and density estimates from the three distributions for TS/ECE discrepancy Pulse No: 62695 are shown as well as the ECE temperature measurements for comparison. It illustrates that the non-Maxwellian bulk temperature is typically 10% higher than the Maxwellian whereas the Lorentzian is ≈ 40% lower, where we recall that the bulk T_e^* is used for the Lorentzian. The reason for the large deviation between the Lorentzian and Maxwellian temperatures is because of the κ value of five used for the spectral index, creating a very large high energy population. Since the Lorentzian chi-square values are much larger than the Maxwellian for ohmic conditions, it indicates that the Lorentzian is clearly not the best fit and the Lorentzian temperatue estimates are inaccurate. However, at high heating levels, the Lorentzian and Maxwellian chi-square values are quite similar but there are still large deviations between the temperature estimates. This provides further evidence that it is not possible to consistently distinguish between the two distributions at high temperatures using the LIDAR data.

Figure 18(b) shows the fitted density estimates relative to the Maxwellian values. It can be seen that larger deviations compared to the Maxwellian values are observed for both distributions during the high heating phase, again because the tail of the scattered spectrum has been removed, removing constraints on temperature and density parameters.

The results also show that if a tailed electron distribution was present in the plasma then fitting a Maxwellian to the data would only cause one to overestimatethe temperature and since the ECE temperature is observed to be 15-20% higher than the TS, the discrepancy cannot simply be caused by the effect of a high energy tail on the TS measurements. Only a distortion to the low energy region would improve agreement between ECE and TS measurements as shown in Figure 18(a), where the non-Maxwellian bulk temperature estimates are closer to the ECE measurements than the Maxwellian.

It is also worth highlighting that there is an apparent TS/ECE discrepancy at low temperatures in the time period 0-5s, while the LHCD is on and before the NBI + ICRH are applied. This is caused by a population of suprathermals generated by the LH heating. Under these conditions, the plasma is optically thin and the suprathermals cannot be reabsorbed by the plasma leading to a distortion to the ECE spectrum. In this case, what is measured is the superposition of the second harmonic thermal emission from the core with the third harmonic emission of the suprathermals located at the edge and will thus cause an increased peak central temperature value. However, once the NBI + ICRH are applied, the optical thickness is large enough so that any suprathermals are reabsorbed by the plasma and have no influence on the core ECE measurements [7].

It must be stated that the temperature results presented here may not be meaningful for such non-Maxwellian distributions, where thermodynamic equilibrium is no longer applicable and therefore, the scattering volume cannot be represented by a single temperature.

5. CALIBRATION ANALYSIS

As mentioned previously, calibration inaccuracies have been suggested as a possible cause of the discrepancy and in this section, the accuracy of the LIDAR system for a number of the shots is investigated to determine if any calibration issues can be identified and if these could be related to the TS/ECE discrepancy. As part of this investigation, the measured chi-square distribution and the fitting residuals are analysed.

It is clear that noise is introduced into the detected signals due to statistical fluctuations in the Thomson scattered signals and from plasma background light generated from stray laser light and other forms of radiation including Brehmstrahlung. Plasma light contributions can be particularly significant in broad spectral channels. Additional noise is also created within the detector/amplifier system, which can dramatically reduce the signal-to-noise ratio in narrow spectral bands or in channels with a low scattered signal. This noise will in turn induce errors in the temperature and density estimations. The noise is estimated and used for the signal standard deviation, σ_i of each channel in the fitting routine.

Two sample Maxwellian fitted spectra are shown in Figure 19 for Pulse No's: 69300, a purely ohmic shot, and 62695, a high performance shot with an observed TS/ECE temperature discrepancy.

Since each fit is performed with two parameters using six data points, there are four degrees of freedom. In general, a χ^2 approximately equal to the number of degrees of freedom is expected. If the value of the χ^2 is too low then the error estimates on the signals are too large. On the other hand, if it is too high then either the error estimates are too conservative or the underlying fitting function is not accurate. The resultant unnormalised χ^2 values for the above fits are 9.94 and 6.74 for Pulse No's: 69300 and 62695, respectively. It can also be seen that the fitted signals are often outside the experimental signal error estimates. It is necessary to examine the distribution of chi-squares for a larger number of fits as well as the fitting residuals to make further conclusions.

The measured χ^2 distribution over a large number of shots, with central temperatures varying from 2keV (ohmic) to 10 keV (NBI+ICRH), is plotted in Figure 20. The theoretical chi-square distribution for a system with 4 degrees of freedom is superimposed and and is inconsistent with the measured distribution. This shows that the measured chi-square values are typically greater than the number of degrees of freedom, indicating that either the error estimates on the signals are too conservative or the fitting function may be inaccurate in some way. The fitting residuals for Pulse No: 62695 at the centre radial point are shown in Figure 21, where the left-hand set of graphs show the experimental and Maxwellian fitted signals and the right-hand set show the residuals as well as the mean residual value.

In general, the residuals should consist of random fluctuations about the zero point. However,

Figure 21 shows that systematic deviations are observed in many of the spectral channels. For example, the theoretical signals in channel 1 are consistently higher than the experimental values, with a mean residual of −5.686. The residuals in channel 2 show that the fitted signals are lower than those actually received with an average value of + 15.5. Channels 5 and 6 also show consistent deviations between the experimental and fitted signals. These results combined with the measured chi-square distribution would indicate some calibration inaccuracies.

Further examination of the experimental signals shows that channel five has consistently negative signal levels at the start and end of the shot. This occurs because at these times the temperatures/densities are low and so the signals in the high energy channels will be low. In addition, the level of background light may be overestimated and so when subtracted, the result can be negative. The background light can be overestimated as it is calculated before the laser pulse enters the plasma and assumed equal to that value while scattering occurs, which may not be the case. It was also noticed that for later shots, an issue with stray light at the detectors was causing channel one to become largely negative, although this is not apparent from the TS signals for Pulse No: 62695.

To understand the effect of negative signal levels in channel five at low temperatures, the temperatures estimates based on Maxwellian fits, for Pulse No's: 69300 and 75100 without using channels five and six were determined as shown in Figure 22. The temperature results show that the estimations using all the available channels are consistently lower ($\approx 7-8\%$) than those without channels five and six. Further fits were performed for Pulse No: 69300, firstly without channel five and secondly, without channel six used. The results showed that the signal fits without channel six give identical temperature estimates to those when all channels are used, whereas, the fits without channel five provide consistently higher temperature values. This would imply that the overestimation of the background light in channel five, leading to negative signal levels in Pulse No: 69300, is causing the temperature to be underestimated at low temperatures.

So far this section has highlighted possible calibration errors with the LIDAR system and that an overestimation of the background light in channel five is causing an underestimation of the electron temperature at low temperatures. Work is now carried out in an attempt to improve the calibration of LIDAR system, determine the effect of the background light issue with channel five on discrepancy Pulse No: 62695 and therefore on the TS/ECE discrepancy in general.

Attempts were made to improve the spectral calibration by altering the sensitivities of the spectral channels for high performance Pulse No: 62695 based on the fitting residuals. In order to determine the effect of the issue with channel five, it was decided to remove channel five from the fit. Extra photoelectrons could have been added to channel five to negate the effect of the overestimated background light but the number of photoelectrons added would be somewhat arbitrary. In addition, it was decided to remove channel one from the fits as the overfitting of the data would indicate that the stray light issue affecting later shots was also influencing Pulse No: 62695, although not as significantly. The spectral transmission of the four remaining channels were then modified (by a maximum of 5%) to ensure that the resultant signal residuals had mean values as close to zero as

possible. The residuals for Pulse No: 62695, with modified calibration values, are shown in Figure 23 with a clear improvement in the mean residual values.

The temperature estimations from Maxwellian fits with both new and old calibrations, as well as the ECE temperature measurements, are shown in Figure 24 for Pulse No: 62695. The results show that at low temperatures the same results as the ohmic case above are obtained, i.e. when channel five is used in the fit, the temperature is underestimated by $\approx 7-8\%$. However, at high temperatures, the removal of channel five from the fit has a negligible effect, this is because at high temperatures the signal in channel five is large and so the subtraction of the background light from channel five will not produce a significant change in the signal level. Also at high temperatures, the signal in channel six will typically be larger than in channel five (see Figure 6) and so channel six will dominate in the fit. The effect of removing channel one and altering the spectral sensitivity appeared to cause negligible changes to the temperature estimates.

The chi-square analysis was repeated with the new calibration but unfortunately no improvement in the results was achieved as the model remained unable to identify the best fit during the heating stage for Pulse No: 62695. This may provide further evidence that it is necessary to measure the tail of the spectrum to determine the electron distribution. Although it must be pointed out that the calibration corrections were purely based on the fitting residuals and perhaps a more accurate procedure is required for such corrections and may produce an improvement in the chi-square results.

The analysis presented here, shows that although minor calibration issues have been identified for Pulse No: 2695, causing slight inaccuracies at low temperatures, it appears that such calibration errors in the LIDAR system are not related to the temperature discrepancy. A re-calibration was performed at Pulse No: 63700, which appears to have resolved any errors in the spectral transmissions but the background light in channel one and five remain overestimated in some cases. Work should be carried out to remove overestimations of background light to improve accuracy at low temperatures.

6. CONCLUSIONS

In this paper, the core LIDAR TS diagnostic at JET was used in an attempt to detect the presence of non-Maxwellian distributions for a number of high performance discharges. A technique to examine non-Maxwellian behaviour by monitoring chi-square values from fits based on non-Maxwellian distributions has been presented. A non-Maxwellian bulk [3] and a generalized Lorentzian distribution function [5] were used as the non-Maxwellian distributions, where the non-Maxwellian bulk distribution represents a distortion to the low energy part of the Maxwellian and the Lorentzian represents a high energy tailed distribution. It was found that basing conclusions on the resultant fits from data for a single time and radial point can be misleading due to the noisiness in the LIDAR data. Instead it is necessary to evaluate the chi-square values over the entire duration of the LIDAR measurement period.

Several cases, which can be regarded as representative of experiments at JET, where a TS/ECE temperature measurement discrepancy has been observed were analysed. A clear change in the chi-square behaviour was observed for both the non-Maxwellian bulk and Lorentzian distribution functions on the application of high auxiliary heating, where it was not possible to consistently identify the best fit distribution. After numerous inconclusive results, similar chi-square behaviour was observed for non-discrepant cases with high heating levels, which would imply that this change in the chi-square behaviour is not related to the TS/ECE discrepancy. The analysis was also carried out on purely ohmic shots and the evidence of non-Maxwellian behaviour was not found in any case. Further analysis suggested that it is not possible to distinguish between the distributions at high temperatures using the LIDAR data as the tail of the scattered spectrum is not measured at high temperatures. This suggests that the LIDAR system may need to measure lower wavelengths in order to identify the electron distribution.

The temperature estimations from fits based on the non-Maxwellian bulk and Lorentzian distributions were also recorded. As expected the non-Maxwellian bulk temperature is $\approx 10\%$ higher than the Maxwellian whereas the Lorentzian is $\approx 40\%$ lower for $\kappa = 5$. The results show that the presence of a high energy population will cause one to overestimate the electron temperature and therefore the TS/ECE discrepancy cannot simply be caused by the effect of a high energy tail on the LIDAR TS measurements as the ECE temperature is observed to be 15-20% higher than the TS. The temperature estimates based on the non-Maxwellian distribution function are much closer to the ECE temperatures than the Maxwellian, which would suggest that if the TS/ECE discrepancy is caused by the effect of a distorted Maxwellian on the TS system, only a distortion to the low energy part would resolve the discrepancy. However, it must be reiterated that the temperature results may not be meaningful for such non-Maxwellian distributions, where thermodynamic equilibrium is no longer applicable.

The accuracy of the LIDAR TS system was then analysed by monitoring the chi-square distribution over a large number of fits and it was discovered that the distribution of chi-squares does not represent that of a system with four degrees of freedom. In addition, the fitted signals were often outside the signal error estimates. This suggested that either the error estimates are too conservative or the actual fitting function used does not represent the data. Non-random fluctuations in the fitting residuals provided further evidence of some minor calibration inaccuracies. In addition, a potential problem with channel five, where an overestimation of the background light causes negative signal levels in channel five at low temperatures was identified. The consequence of this problem and the calibration inaccuracies on the temperatures estimates were then analysed for the TS/ECE discrepancy Pulse No: 62695. It was found that the temperature was underestimated by $\approx 7-8\%$ at low temperatures but its effect is negligible high temperatures. This would imply that any calibration errors in the LIDAR system are not related to the ECE/TS discrepancy observed at high temperatures. The chi-square analysis was also repeated for Pulse No: 62695 using the new calibrations but unfortunately no improvement on the previous results was achieved, providing evidence that it may be required to

measure the a larger portion of scattered spectrum in order to determine the electron distribution.

The work carried out in this paper failed to prove or disprove the presence of non-Maxwellian distributions during strong auxiliary heating at JET using the LIDAR TS diagnostic and therefore a correlation between the TS/ECE discrepancy and non-Maxwellian behaviour was not determined. The calibration analysis performed showed that although some minor errors were identfied in the LIDAR system, they could not explain the TS/ECE discrepancy.

ACKNOWLEDGEMENTS

The main author would like to acknowledge the support of the Irish Research Council for Science, Engineering and Technology for an Embark Initiative Scholarship, which made this work possible. The authors would also like to thank Andreas Dinklage for providing data on the non-Maxwellian bulk distribution function and Adrian Capel for his assistance during the model development. This work was partly supported by the European Communities under the contract of Association between EURATOM and DCU, and was carried out within the framework of the European Fusion Development Agreement. The views and opinions expressed herein do not necessarily reflect those of the European Commission.

REFERENCES

[1]. A.J.H. Donn, A. E. Costley, and et al. Progress in the ITER physics basis, chapter 7:Diagnostics. Nuclear Fusion, **46**, 337–384, 2007.

[2]. V. Krivenski. Electron cyclotron emission by non-Maxwellian bulk distribution functions. Fusion Engineering and Design, **53**, 23–33, 2001.

[3]. V. Krivenski, E. de la Luna, and G. Giruzzi. Evidence of Non-Maxwellian Electron Bulk Distributions on JET. In–29th EPS Conference on Plasma Phys. and Contr. Fusion, volume 26B, Montreux, 17-21 June 2002.

[4]. G. Taylor, E. Fredrickson, B. Grek, and A. Janos. Electron cyclotron emission measurements on high beta TFTR plasmas. In Proc. 9th Joint Workshop on ECE and ECRH. ed. John Lohr, World Scientific, 1995.

[5]. O. Naito, H . Yoshida, T. Hatae, A. Nagashima, and T. Matoba. Relativistic incoherent thomson scattering spectrum for generalized Lorentzian distributions. Phys. Plasmas **3**, 4:1474–1476, 1995.

[6]. E. de la Luna, V. Krivenski, G. Giruzzi, C. Gowers, R.Prentice, J.M. Travere, and M. Zerbini. Impact of bulk non-Maxwellian electrons on electron temperature measurements. Review of Scientific Instruments, **74** (3), 2003.

[7]. E. de la Luna, D. Farina, L. Figini, G. Grosseti, S. Nowak, C. Sozzi, M. Beurskens, O. Ford, T. Johnson, and JET-EFDA contributors. Recent results on the discrepancy between electron temperature measurements in high temperature plasmas in JET. In Proc. of the 15th Joint Workshop on ECE and ECRH, Yosemite (USA), 2008. World Scientific.

[8]. I.H. Hutchinson. Principles of Plasma Diagnostics. Cambridge University Press, 2002.

[9]. J. Sheffield. Plasma Scattering of Electromagnetic Radiation, pages 31,41. Academic Press, 1975.

[10]. H. Salzmann, J. Bundgaard, and A. Gadd et al. The LIDAR Thomson Scattering Diagnostic on JET. Technical report, JET-R(89)07.

[11]. G.W. Gowers, B.W. Brown, H. Fajemirokun, P. Nielsen, Y. Nizienko, and B. Schunke. Recent developments in LIDAR Thomson scattering measurements on JET. Rev. Sci. Instrum., **66** (1), 471–475, 1995.

[12]. P.R. Bevington. Data Reduction and Error Analysis for the Physical Sciences. McGraw-Hill, New York, 1969.

[13]. A. Dinklage and S. Schmuck. Private communications on non-Maxwellian bulk distribution, Greifswald.

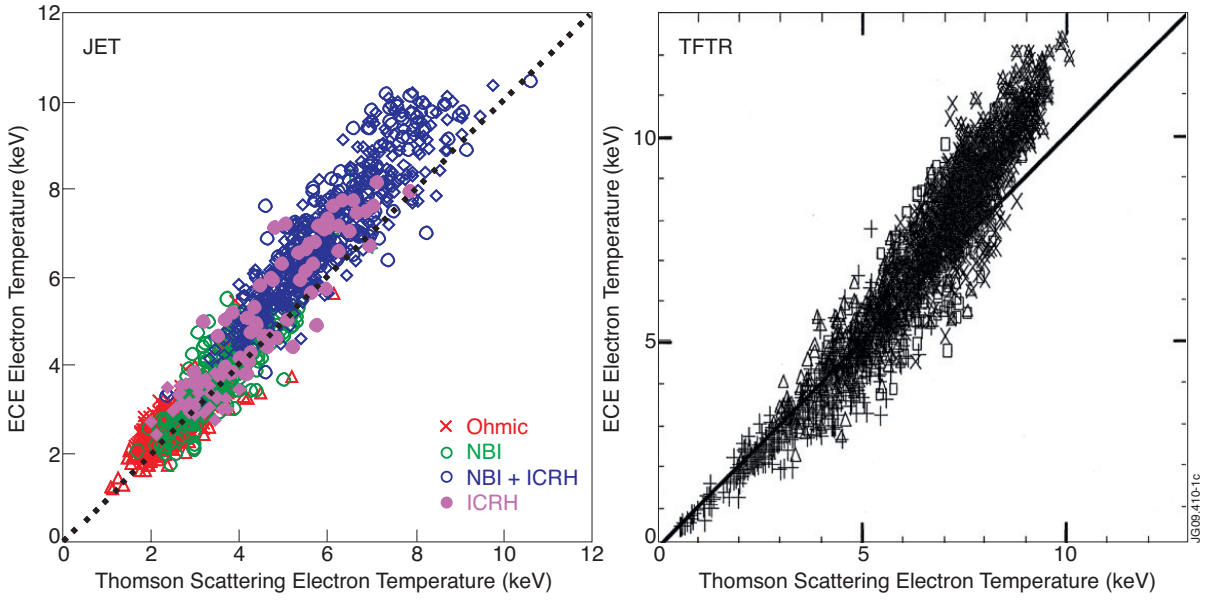

Figure 1: Systematic discrepancies between ECE and Thomson scattering in the central region in high T_e plasmas in JET (Reprinted with permission from [6]) and TFTR (Reprinted with permission from [4])

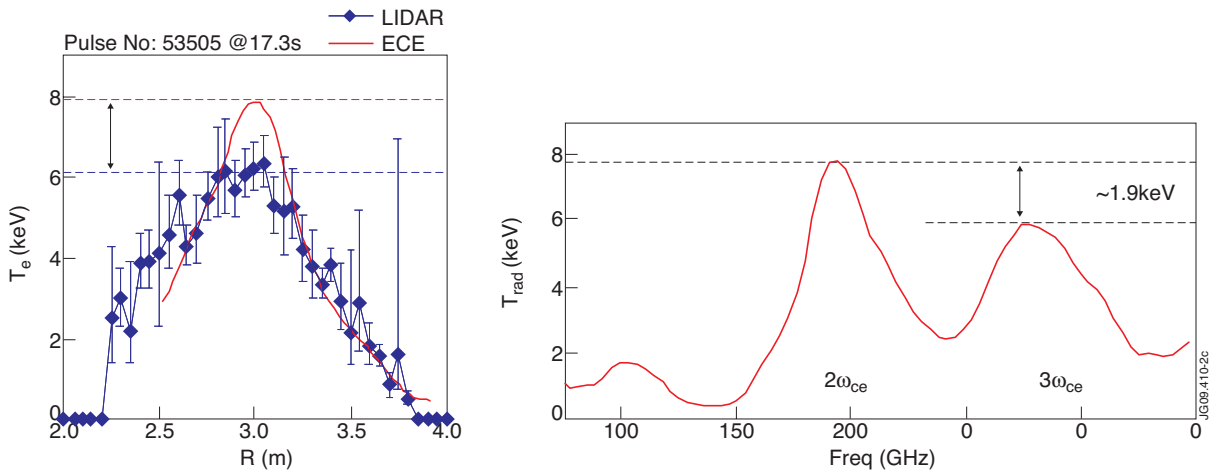

Figure 2: ECE and LIDAR temperature profiles for discrepant Pulse No: 53505 and the corresponding ECE spectrum (Reprinted with permission from [7].

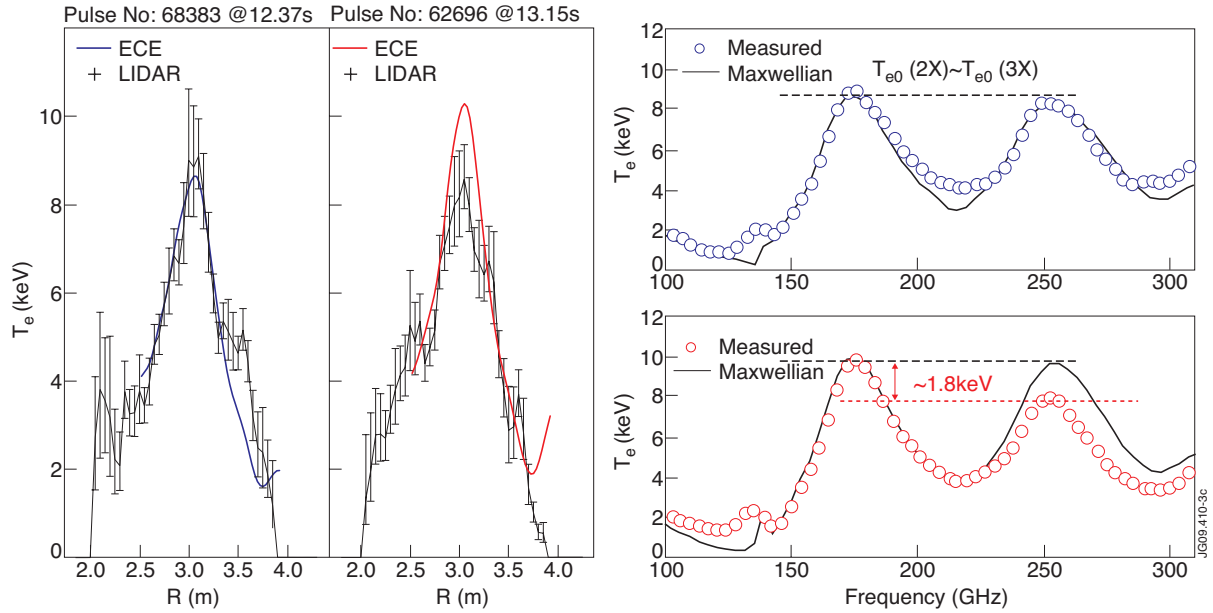

Figure 3: Measured and computed ECE spectra for shots Pulse No's: 68383, 62696 and the corresponding TS and ECE temperature profiles [7].

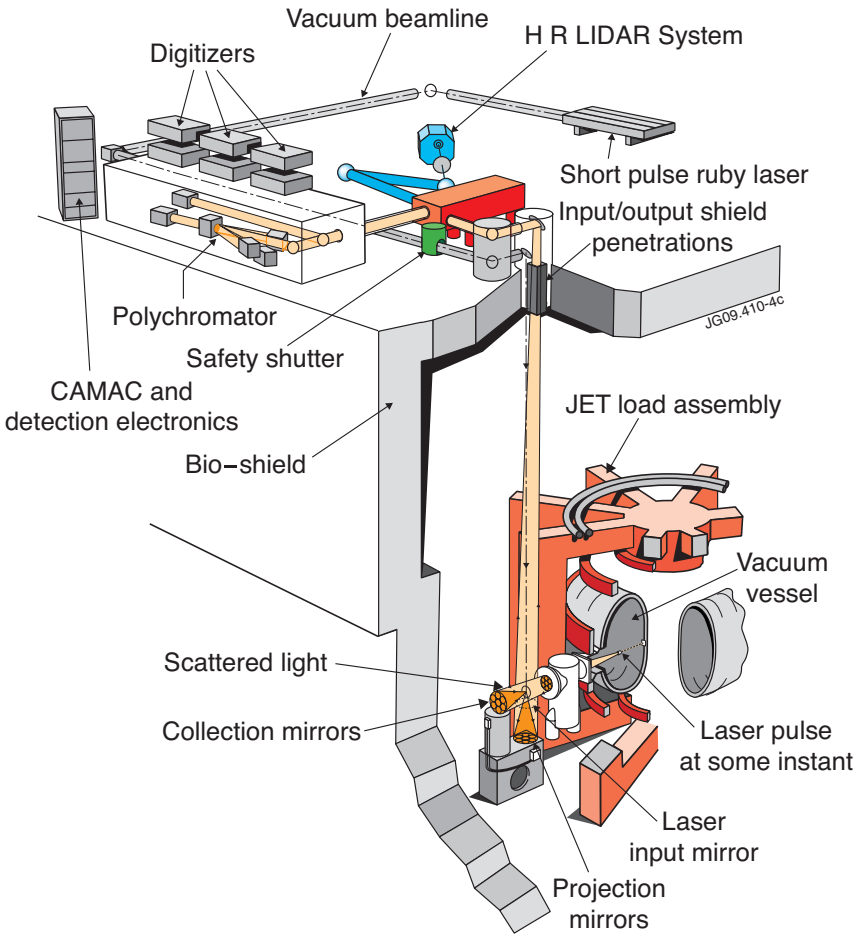

Figure 4: Layout of the core LIDAR TS system [11].

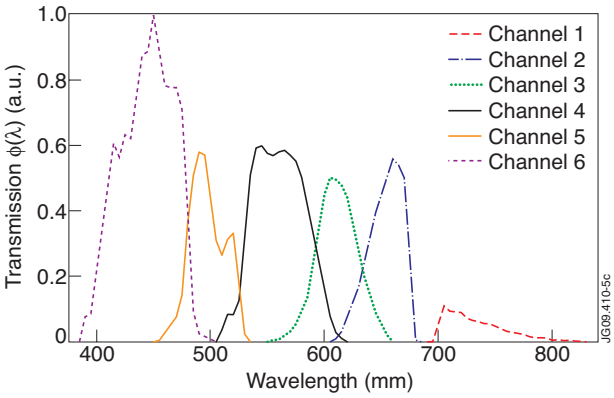

Figure 5: Spectral transmission of the JET core LIDAR TS spectrometer with all filters normalised. The laser wavelength is 694.3nm.

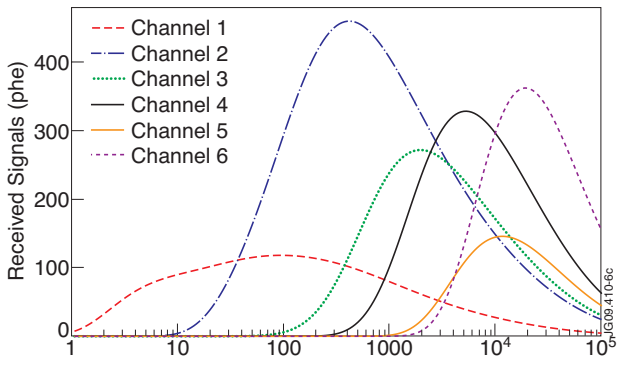

Figure 6: Thomson Scattered signals over a large temperature range for a density of 1×10^{19} m^{-3} in the core LIDAR TS system.

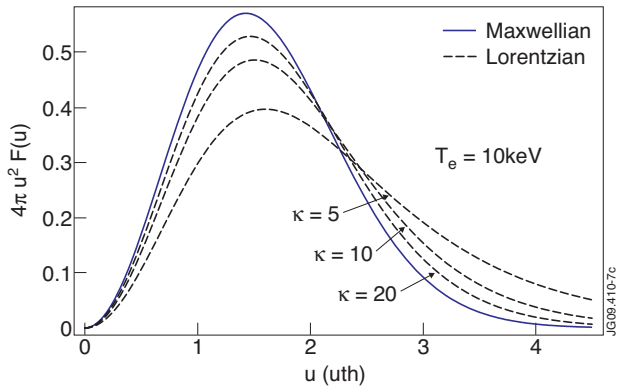

Figure 7: Lorentzian distribution functions at $T_e^* = 10keV$ as a function of normalized momentum $u = p/uth$, $u_{th} = \sqrt{m_e T_e}$.

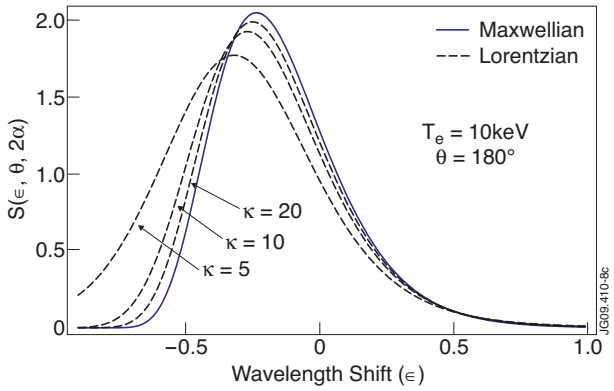

Figure 8: Generalized Lorentzian Spectra at $T_e^* = 10keV$ and $\theta = 180^o$ as a function of wavelength shift ϵ $(= \frac{\lambda_s - \lambda_i}{\lambda_i})$.

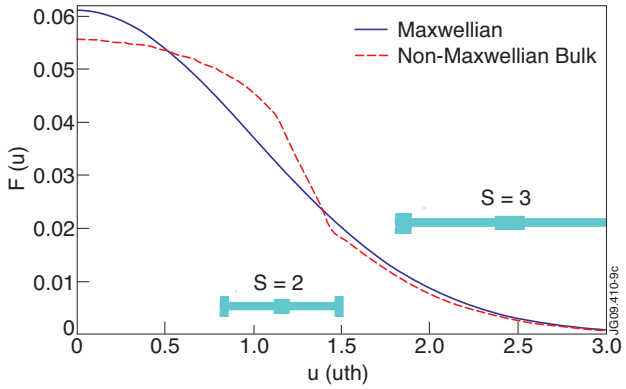

Figure 9: Non-Maxwellian bulk distribution as a function of normalised momentum $u = p/u_{th}$ is shown in comparison to the Maxwellian distribution

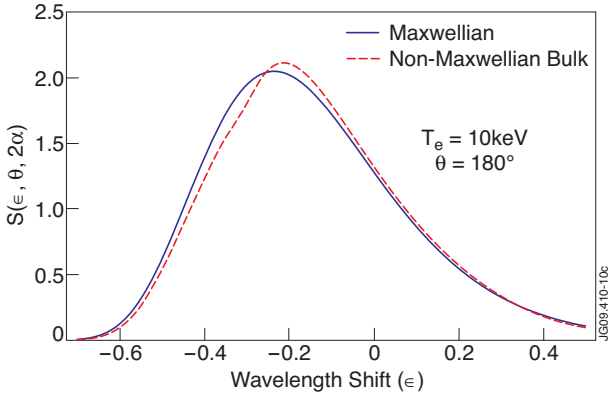

Figure 10: Non-Maxwellian bulk spectrum at $T_e = 10keV$ and $\theta = 180^o$ as a function of wavelength shift ϵ.

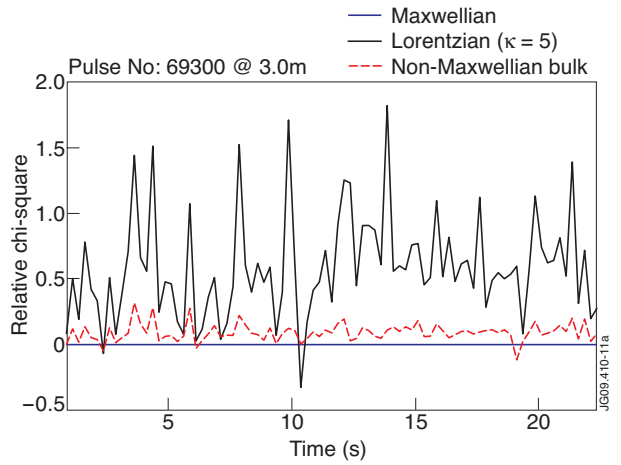

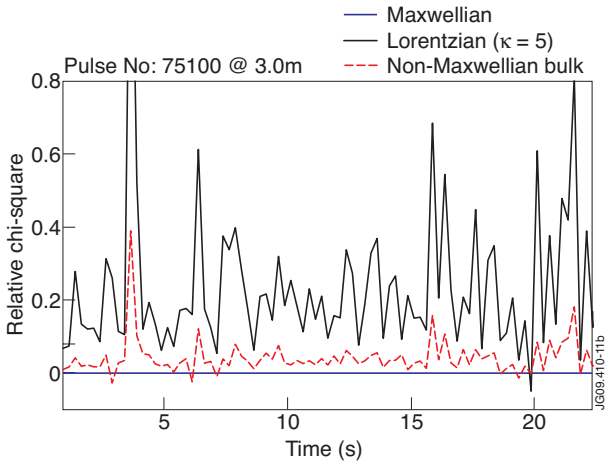

Figure 11: Relative chi-square results for ohmic shots (a) Pulse No: 69300 and (b) 75100, both with plasma current $I_p \approx 2MA$, reaching central temperatures of 2keV and densities of $3\times10^{19}\ m^{-3}$.

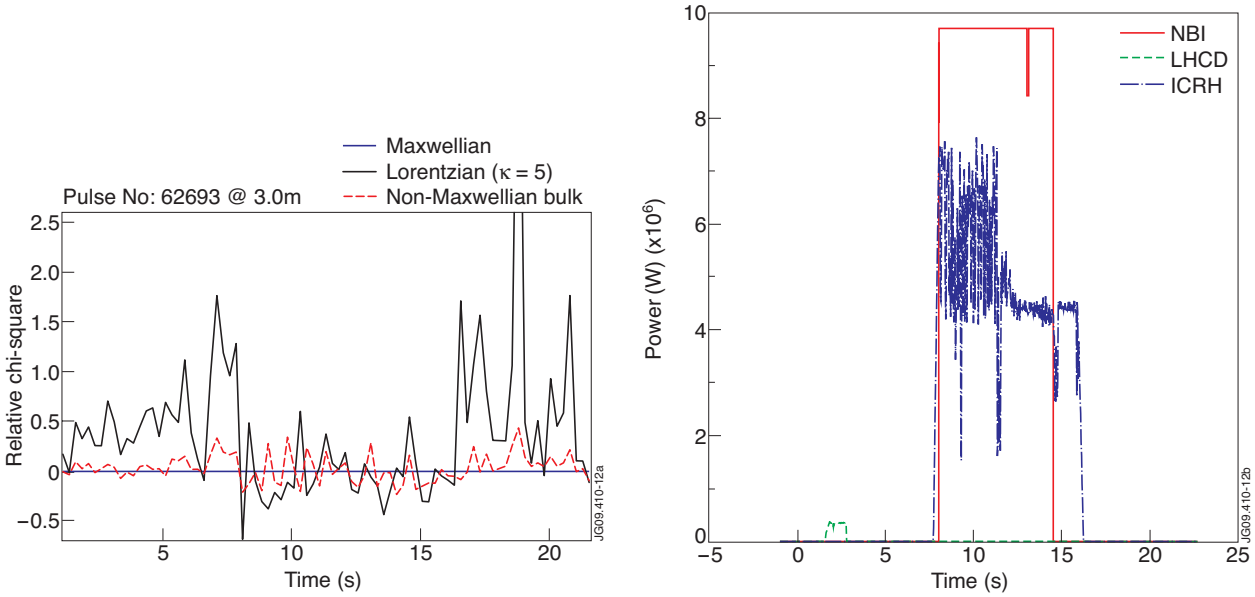

Figure 12: (a) Relative chi-square results for discrepant Pulse No: 62693 and (b) the corresponding auxiliary heating conditions. Central temperatures of ≈ 8keV and densities of 3×10^{19} m^{-3} are reached.

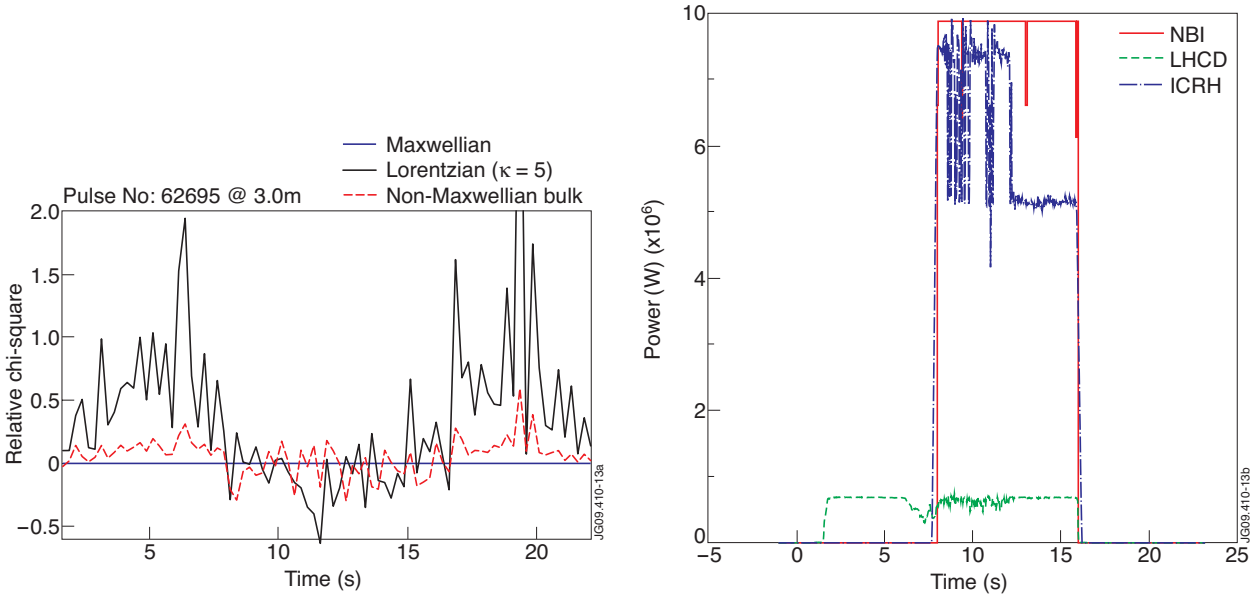

Figure 13: (a) Relative chi-square results for discrepant Pulse No: 62695 and (b) the corresponding auxiliary heating conditions. Central temperatures of ≈ 8keV and densities of 3×10^{19} m^{-3} are reached

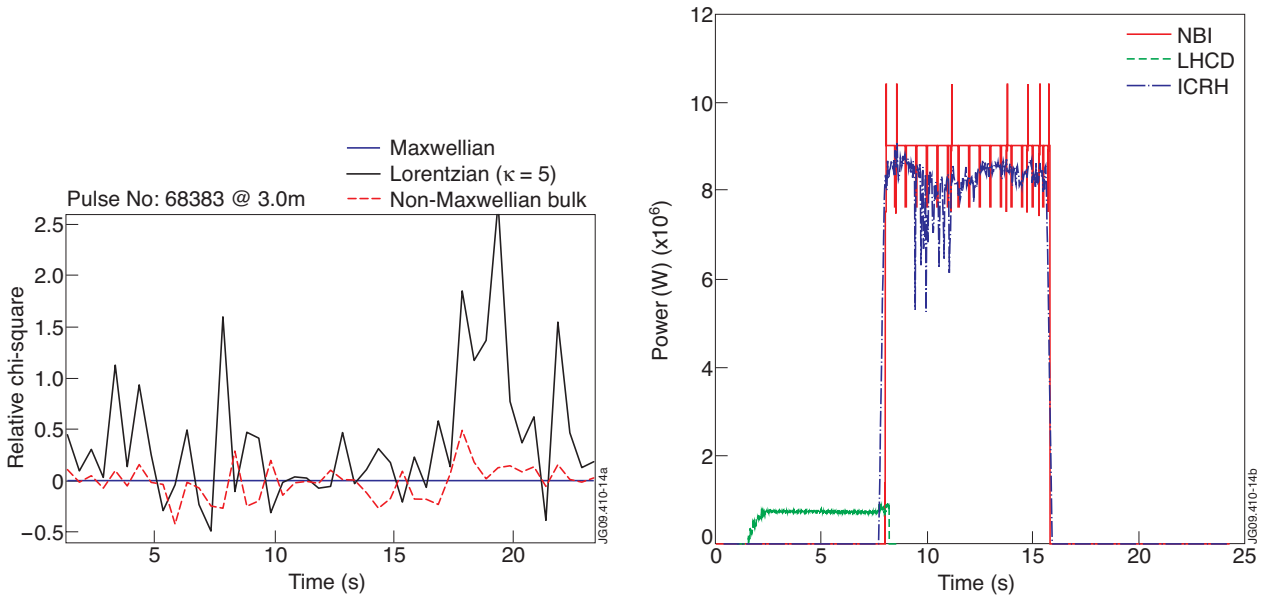

Figure 14: (a) Relative chi-square results and (b) the corresponding auxiliary heating conditions for Pulse No: 68383. Central temperatures of ≈ 9keV and densities of 3×10^{19} m^{-3} are reached

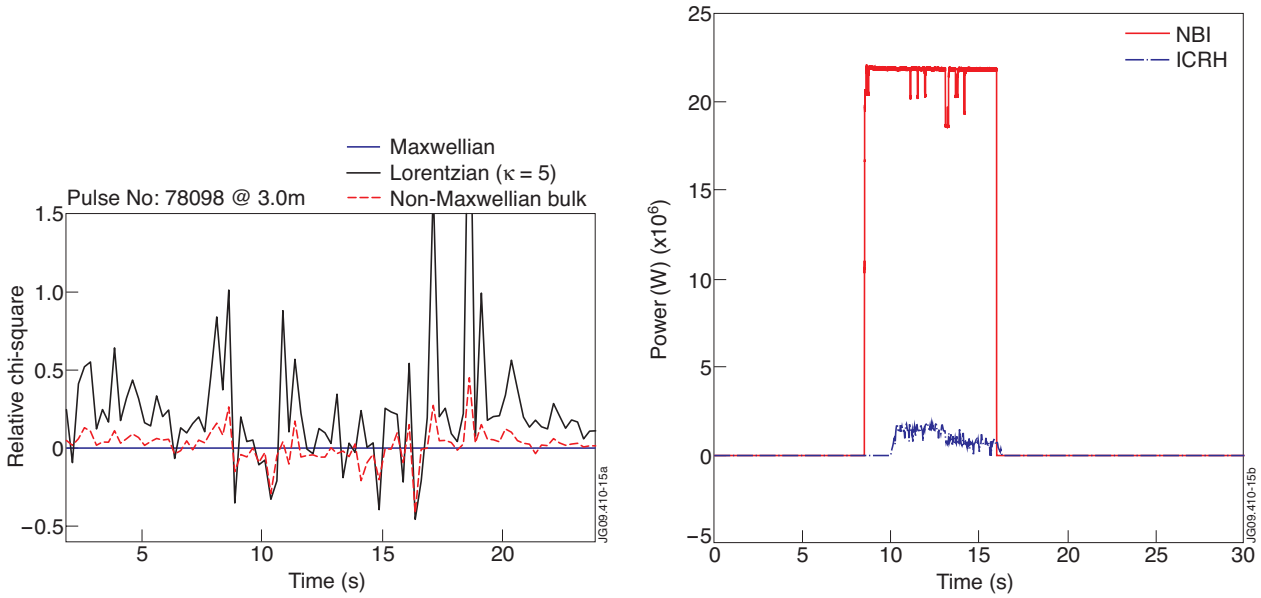

Figure 15: (a) Relative chi-square results and (b) the corresponding auxiliary heating conditions for Pulse No: 78098. Central temperatures of ≈ 6keV and densities of 8×10^{19} m^{-3} are reached

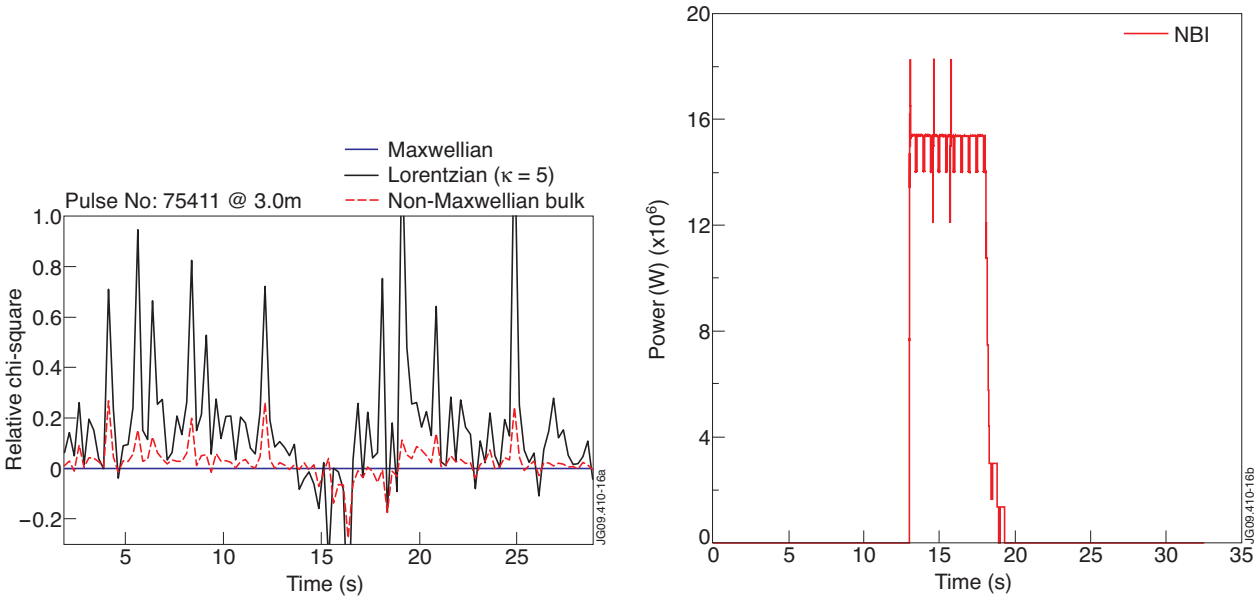

Figure 16: (a) Relative chi-square results and (b) the corresponding auxiliary heating conditions for Pulse No: 75411. Central temperatures of ≈8keV and densities of 8×10^{19} m^{-3} are reached

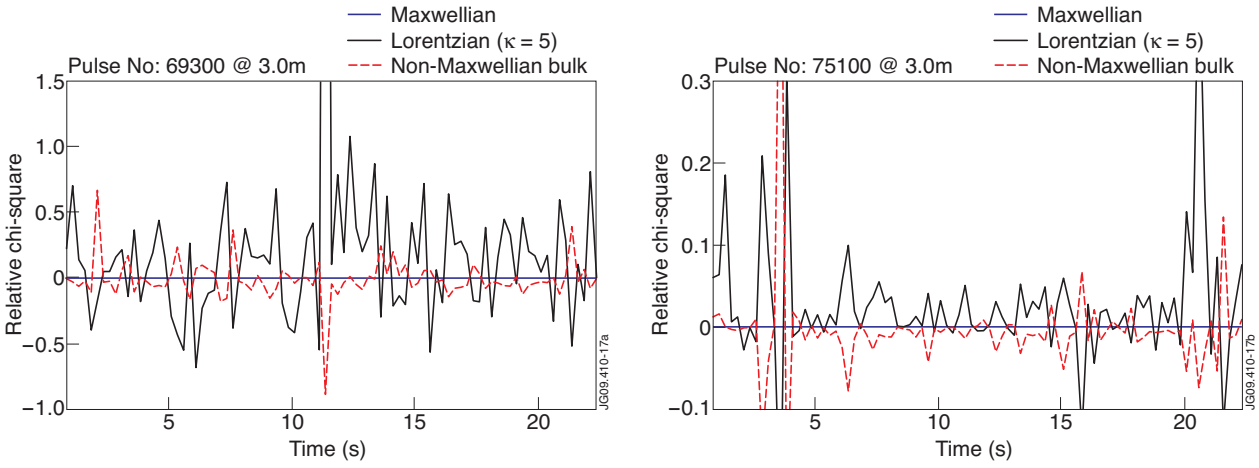

Figure 17: Relative chi-square results for ohmic shots (a) Pulse No's: 69300 and (b) 75100, without spectral channels five and six used in the fits.

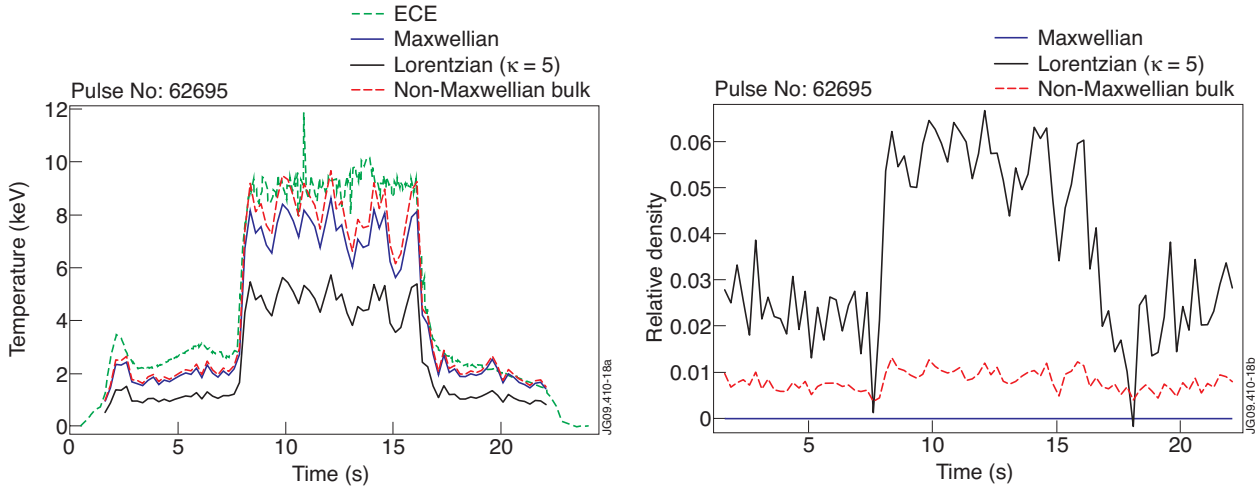

Figure 18. (a) Fitted temperature results and (b) relative fitted density results for discrepant Pulse No: 62695.

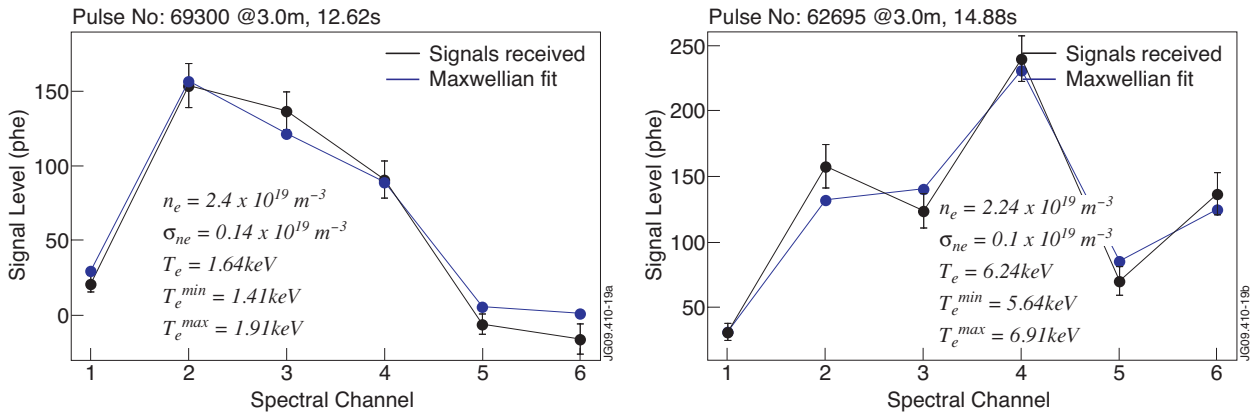

Figure 19. Fits in n_e and T_e to measured scattered signals for (a) Ohmic Pulse No: 69300 and (b) High performance Pulse No: 62695.

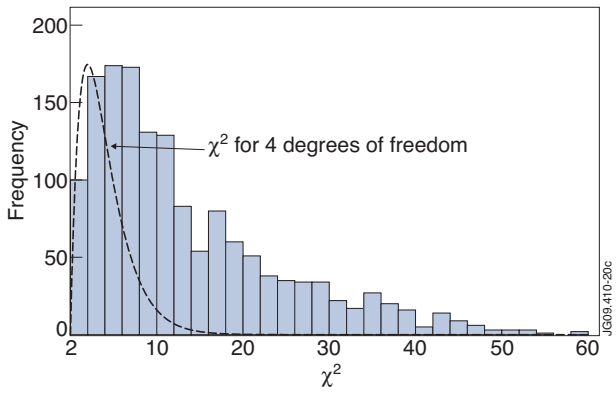

Figure 20: χ^2 measured over a large number of convergences.

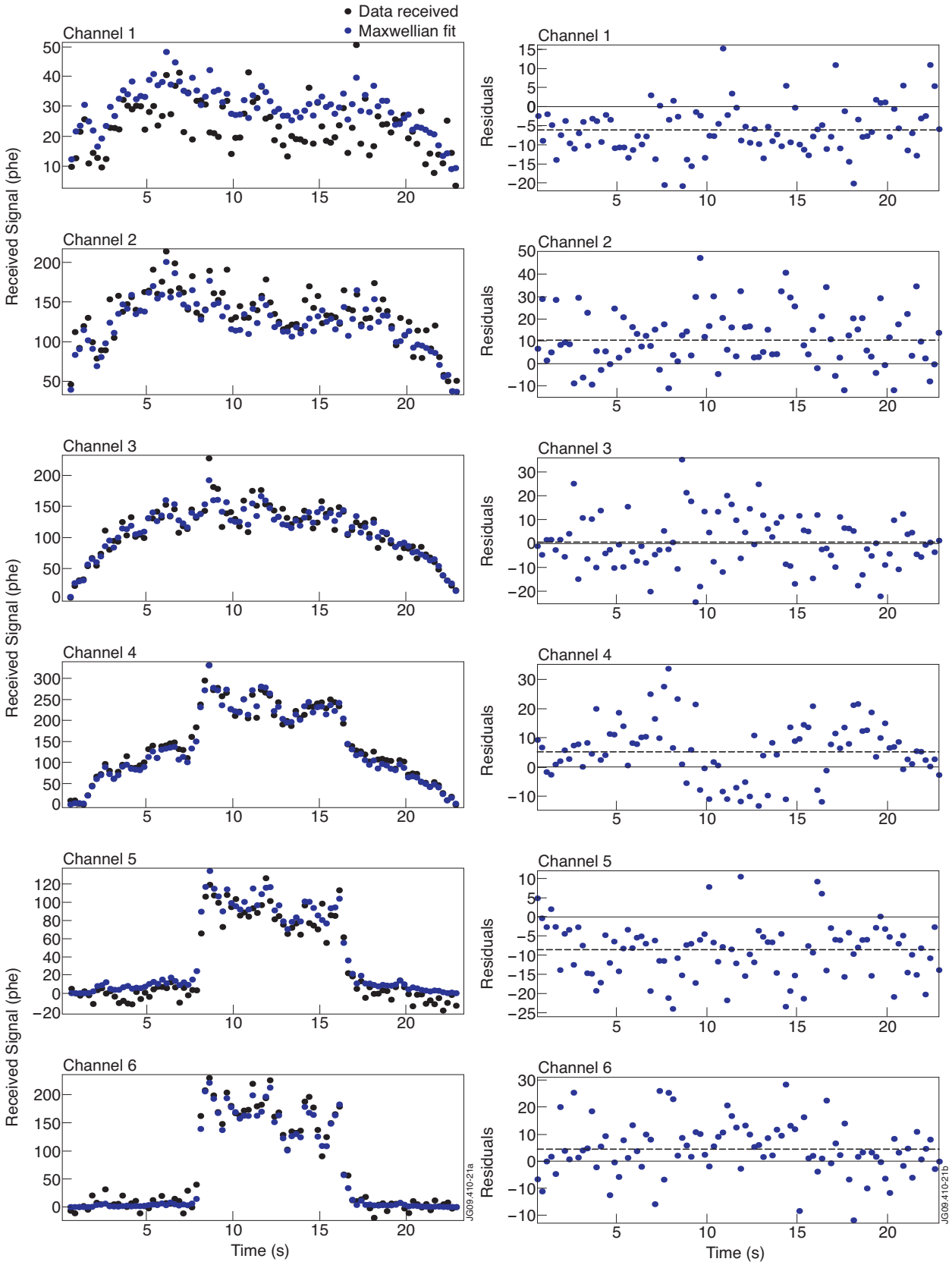

Figure 21: Signal residuals for Pulse No: 62695 at 3.0m with the mean residual value indicated by the black dashed line. The measured and fitted signals are also shown.

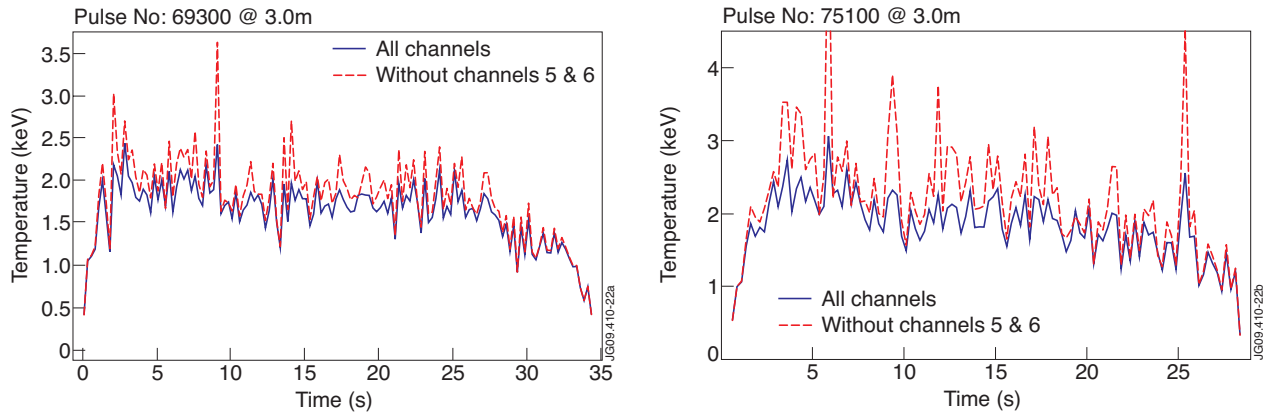

Figure 22: Temperature estimations for ohmic shots (a) Pulse No's: 69300 and (b) 75100, without spectral channels five and six used in the fits.

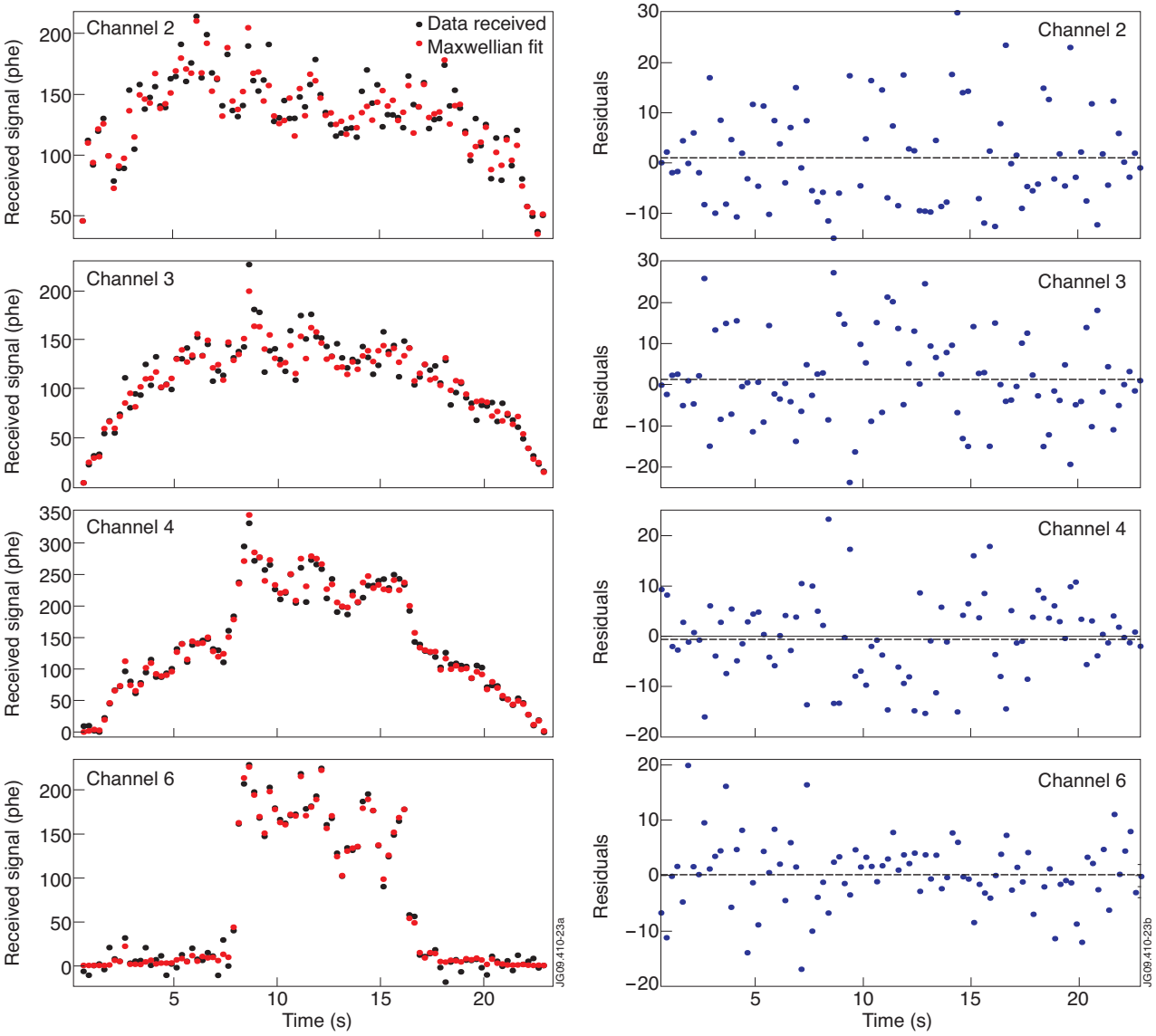

Figure 23: Signal Residuals for Pulse No: 62695 at 3.0m for new calibration

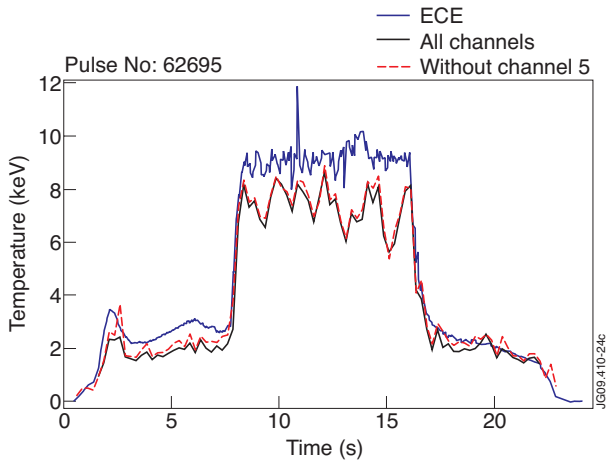

Figure 24. Comparison of temperature estimations for Maxwellian fits using modified spectral channels